Korean J. Chem. Eng., 39(6), 1396-1411 (2022)
DOI: 10.1007/s11814-022-1081-8

pISSN: 0256-1115
eISSN: 1975-7220

Sensitivity analysis for parameter classification of energy balance-integrated single particle model for battery cells

Changbeom Hong*, Se-Kyu Oh, and Yeonsoo Kim*,†**

*Department of Chemical Engineering, Kwangwoon University, 20 Kwangwoon-ro, Nowon-gu, Seoul 01897, Korea
**Electrification Control Development Team 1, Hyundai Motor Company, Hwaesong 18280, Korea
(*Received 31 October 2021 • Revised 6 January 2022 • Accepted 29 January 2022*)

Abstract−With the increasing use of electric vehicles (EVs), there is a growing interest in the thermal management of EVs. In this study, we first reduced the computational complexity of single particle model (SPM) for the battery cell by introducing a 4th order approximation for Li-ion concentration in the solid phase. In addition, by integrating it with an energy balance, the constructed model can calculate the battery temperature along with the terminal voltage and state of charge. To develop a model compatible with the experimental data requires parameter estimation. However, the estimation accuracy for each parameter depends on its sensitivity. We investigated the influence of 16 parameters on the measured data under general experimental conditions (constant C-rate discharge) through simulations and sensitivity analysis. We classified the radius of the particle, total active surface areas, electrode maximum concentration, and a heat transfer coefficient as dominant parameters. When dominant parameters were estimated using the virtual experimental data, the percent error was smaller than 3.1%. For the parameters with minor influence, the estimation error was large even with the excellent agreement of the experimental data. We confirmed which parameter could be estimated using the C-rate experimental data accurately and which parameter should be estimated with additional experiments.

Keywords: Single Particle Model, Battery Temperature, Sensitivity Analysis, Genetic Algorithm, Parameter Estimation

INTRODUCTION

Lithium-ion batteries (LIBs) have a higher energy density than other batteries and a low self-discharge rate [1-4,12,16]. Their performance is affected by the operation temperature; thus, a battery management system is required for better battery operation, and a dynamic model is helpful in the optimization of the system-wide performance [6,8-10,12]. In particular, the dynamic models should have an appropriate computational complexity and accuracy for the model-based control. In addition, an electrical model integrated with energy balance is needed for thermal management.

The equivalent circuit model (ECM) has been widely applied owing to its simple model structure, low computational burden, and easy parameterization process [10,14]. However, it is an empirical rather than a physicochemical-based model and has limitations in representing the physical meaning of parameters. Moreover, owing to the limited model structure of the ECM, the battery operation strategy must be designed with a large safety margin, such as a conservative cut-off value for voltage and current. To address these issues, it is necessary to build a computationally efficient electrochemical model. In addition, it is required to establish an electrochemical-thermal-coupling model for the temperature prediction, which can further improve the energy optimization of electric vehicles (EVs).

The basic electrochemical model of a LIB is the pseudo-two-dimensional model created by Doyle [2]. This model describes the dynamics comprehensively and systematically. However, the pseudo-two-dimensional model has many differential-algebraic equations and is computationally burdensome. Therefore, the computational costs need to be reduced, and a single-particle model (SPM) is proposed [1-6,8,12,15,16]. However, the existing SPM still needs further simplification because it consists of partial differential equations (PDEs). A fourth-order approximation function for the radial changes of lithium-ion concentration in the electrode is introduced in [2,10].

Several studies have integrated the SPM and energy balance [1, 3-9,11,13]. A general method for calculating the cell temperature is to establish the energy balance equation assuming that the temperature distribution inside the cell is uniform. The amount of heat generated by overpotential, endothermic/exothermic heat due to reversible energy, and heat exchange with the ambient environment are generally considered. The heat of mixing and the energy due to the phase change are typically negligible [11]. In [1], to increase the accuracy of the SPM at high currents, ten eigenfunctions are introduced for each electrode, and the ordinary differential equations (ODEs) are solved for each eigenfunction. In [6], electrolyte dynamics are established to describe the high C-rate case. Both approaches increase the computational load. In this study, we integrated the energy balance with the SPM simplified by using the fourth-order approximation for lower complexity.

To use the simplified SPM integrated with an energy balance, it is required to estimate model parameters from experimental data. Before the parameter estimation, it is necessary to confirm whether the parameters can be estimated from the experimental data. In this paper, a sensitivity analysis is performed under the typical experimental condition, constant C-rate discharge, using the parameters

†To whom correspondence should be addressed.
E-mail: kimy3@kw.ac.kr

of Ref [1]. Based on the parameter sensitivity analysis, we determined which parameters dominantly affect the measurements and can be accurately estimated from the data. Using the virtual experimental data generated by the model, we validated parameter estimation accuracy. Furthermore, we proposed possible additional experiments for the parameter set that has minor effects on the constant C-rate data and cannot be discriminated from the data.

The rest of paper is as follows: In Section 2, we introduce the conventional SPM and the reduced SPM with the detailed governing equations. Section 3 presents the simulation results for selecting main factors for sensitivity analysis, and the results. The estimation results of dominant and minor parameters using virtual experimental data are shown in Section 4. Finally, Section 5 concludes this paper. The detailed nomenclatures are shown in the section after the conclusion.

CONTROL-ORIENTED MODEL FOR BATTERY CELL

1. Conventional SPM

In the SPM, each electrode is assumed to comprise multiple uniform-sized spherical particles, and the current distribution is uniform across the thickness of the porous electrode [1-3,6,8,11]. Based on this assumption, the electrode can be considered a single sphere. Li-ions are stored in the internal porous region of each electrode. A redox reaction occurs at the surface. In addition, a liquid electrolyte is filled in the porous part of the electrodes and between the negative electrode and the positive electrode. The schematic representation is shown in Fig. 1.

The lithium-ion mass balance in the single particle of the electrode active material is described in Eq. (1) by Fick's law in the spherical coordinate system,

$$\frac{\partial c_{s,j}}{\partial t}=\frac{D_{s,j}}{r^2}\frac{\partial}{\partial r}\left(r^2\frac{\partial c_{s,j}}{\partial r}\right)\quad (j=n,\ p) \tag{1}$$

with Neumann boundary conditions as

$$\begin{cases} -D_{s,j}\dfrac{\partial c_{s,j}}{\partial r}=0 & (\text{at } r=0)\\ -D_{s,j}\dfrac{\partial c_{s,j}}{\partial r}=j_j & (\text{at } r=R_j). \end{cases} \tag{2}$$

Here, j_j denotes the molar flux of lithium ions on the surface.

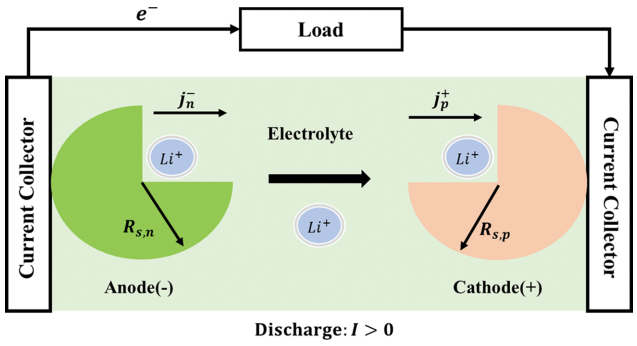

Fig. 1. Schematic representation of the SPM during discharge process.

$$j_p=\frac{I}{F\cdot S_p}\quad j_n=\frac{I}{F\cdot S_n} \tag{3}$$

$$S_j=\frac{3\varepsilon_j V_j}{R_j} \tag{4}$$

In Eq. (3), p and n denote positive and negative electrodes, respectively. I is the total current through the cell, and the positive current represents the discharging process. S_j is the total electroactive surface area of the electrode j. ε_j is the volume fraction of solid phase active material in electrode j. V_j is the total volume of the electrode. The diffusion coefficient $D_{s,j}$ is temperature-dependent based on the Arrhenius equation [1,3,5,6-9,13,15],

$$D_{s,j}(T)=D_{s,j,ref}\exp\left[\frac{Ea_{d,j}}{R}\left(\frac{1}{T_{ref}}-\frac{1}{T}\right)\right]\quad (T_{ref}=298.15\ \text{K}) \tag{5}$$

2. SPM Reduction

The SPM comprising PDEs is further simplified in [2,10]. To describe the dynamics properly even at a high C-rate, a fourth-order approximation of Eq. (6) is introduced for the lithium-ion concentration of the solid phase [2,10].

$$c_{s,j}(r,t)=A(t)+B(t)\left(\frac{r}{R_j}\right)^2+P(t)\left(\frac{r}{R_j}\right)^4 \tag{6}$$

The simplification reduces the PDE of Eq. (1) into the ODEs of Eqs. (7) and (8). The first boundary condition in Eq. (2) is automatically satisfied and the second boundary condition is reflected into Eq. (9). Brief derivations of Eqs. (7)-(10) are shown in the Appendix.

With the simplification of Eq. (6), the dynamics of volume-averaged concentration $\bar{c}_j(t)$ and lithium-ion flux $\bar{q}_j(t)$ are finally used with a low calculation load.

$$\frac{d}{dt}\bar{c}_j(t)=-\frac{3j_j}{R_jF} \tag{7}$$

$$\frac{d}{dt}\bar{q}_j(t)=-30\frac{D_{s,j}}{R_j^2}\bar{q}_j(t)-\frac{45}{2}\frac{j_j}{R_j^2}. \tag{8}$$

The electric current is generated by an electrochemical reaction where lithium ions on the surface participate, and the electrode surface concentration $\bar{c}_{se,j}$ is the concentration in the solid phase at $r=R_j$. From the boundary second condition of Eq. (2), the following expression is obtained,

$$\bar{c}_{se,j}=c_{s,j}(R_j,t)=\bar{c}_j+\frac{8}{35}R_j\bar{q}_j-\frac{1}{35}\frac{j_jR_j}{D_{s,j}} \tag{9}$$

Finally, the time-varying parameters, A(t), B(t), and P(t), are expressed as follows, by using the notations for the volume-averaged concentration, volume-averaged molar flux, and surface concentration. See Eqs. (A3), (A5), and (A7) in the Appendix.

$$\begin{aligned} A(t)&=\frac{39}{4}\bar{c}_{se,j}-3\bar{q}_j(t)R_j-\frac{35}{4}\bar{c}(t)\\ B(t)&=-35\bar{c}_{se,j}+10\bar{q}_j(t)R_j+35\bar{c}(t)\\ P(t)&=\frac{105}{4}\bar{c}_{se,j}-7\bar{q}_j(t)R_j-\frac{105}{4}\bar{c}(t) \end{aligned} \tag{10}$$

Note that SOC in each electrode is calculated as the average lithium-ion concentration divided by the maximum lithium-ion con-

centration [8,10].

$$SOC_j(t) = \frac{\bar{c}_j}{c_{s,j,max}} \quad (11)$$

3. Overpotential

The electrochemical reaction for lithium-ion intercalation/deintercalation at the solid/electrolyte interface can be expressed as follows:

$$Li - \Theta_s \leftrightarrows Li^+ + e^- + \Theta_s \quad (12)$$

where Θ_s represents the empty site on the active surface. The molar flux of lithium ions on the surface, j_j, is related to the electrode surface concentration, electrolyte concentration, and overpotential, which is expressed by Butler-Volmer equation,

$$j_j = k_j c_e^{\alpha} (c_{s,j,max} - \bar{c}_{se,j})^{\alpha} \bar{c}_{se,j}^{\alpha} \left(\exp\left(\frac{(1-\alpha)F\eta_j}{RT}\right) - \exp\left(\frac{-\alpha F\eta_j}{RT}\right) \right) \quad (13)$$

k_j denotes a reaction rate constant based on the Arrhenius equation [1,3,5,6-9,13,15],

$$k_j(T) = k_{j,ref} \exp\left[\frac{Ea_{r,j}}{R}\left(\frac{1}{T_{ref}} - \frac{1}{T}\right)\right] \ (T_{ref} = 298.15\ K). \quad (14)$$

The electrolyte concentration in the solution phase c_e is assumed to be constant [1,5,9]. α is the transfer coefficient, which is set as 0.5 in general. The overpotential η_j is expressed as

$$\eta_p = \frac{2RT}{F}\sinh^{-1}\left(\frac{j_p}{2i_{0,p}}\right), \quad \eta_n = \frac{2RT}{F}\sinh^{-1}\left(\frac{j_n}{2i_{0,n}}\right) \quad (15)$$

with the exchange current,

$$i_{0,j} = k_j(T) c_e^{0.5} (c_{s,j,max} - \bar{c}_{se,j})^{0.5} \bar{c}_{se,j}^{0.5} \quad (16)$$

4. Terminal Voltage

The open-circuit voltage (OCV) is the voltage with no external load, usually measured as the steady-state open-circuit terminal voltage at various SOC points. The regression equations of the OCV used in [1] are as follows:

$$\begin{aligned} U_p = {} & 4.04596 + \exp(-42.30027 \cdot SOC_p + 16.56714) \\ & - 0.04880 \arctan(50.01833 \cdot SOC_p - 26.48897) \\ & - 0.05447 \arctan(18.99678 \cdot SOC_p - 12.32362) \\ & - \exp(78.24095 \cdot SOC_p - 78.68074) \end{aligned} \quad (17)$$

$$\begin{aligned} U_n = {} & 0.13966 + 0.6829\exp(-49.20361 \cdot SOC_n) \\ & + 0.41903 \exp(-254.40067 \cdot SOC_n) \\ & - \exp(49.97886 \cdot SOC_n - 43.37888) \\ & - 0.028221 \arctan(22.52300 \cdot SOC_n - 3.65328) \\ & - 0.01308 \arctan(28.34801 \cdot SOC_n - 13.4396) \end{aligned} \quad (18)$$

$$OCV(SOC) = U_p(SOC_p) - U_n(SOC_n) \quad (19)$$

When a load is placed on the battery, a potential drop occurs because lithium ions pass through the electrolyte between the positive and negative electrodes. This can be considered with the internal resistance R_{cell} rather than with the complex mass and charge transfer dynamics for the lithium-ion concentration on the electrolyte side [1,3,14]. R_{cell} is expressed as Eq. (21), and the exact parameter values will be shown in the next section.

$$\phi_{2,p} - \phi_{2,n} = IR_{cell} \quad (20)$$

$$R_{cell}(T) = \theta_1 (T - T_{amb}) + \theta_2 \quad (21)$$

where $\phi_{2,p}$ and $\phi_{2,n}$ represent solution phase potentials of the positive and negative electrodes, respectively. θ_1 and θ_2 are parameters that vary depending on the ambient temperature and applied current, respectively.

Additionally, the overpotential drop occurs because of the charge transfer and polarization resistance. It is affected by the diffusion and electrochemical reaction rate, as shown in Eq. (15).

Finally, the terminal voltage of the cell is the potential difference between the anode and the cathode,

$$\begin{aligned} V &= \phi_{1,p} - \phi_{1,n} = (\eta_p + \phi_{2,p} + U_p) - (\eta_n + \phi_{2,n} + U_n) \\ &= \left(\sinh^{-1}\left(\frac{j_p}{2i_{0,p}}\right) - \sinh^{-1}\left(\frac{j_n}{2i_{0,n}}\right)\right) \\ &\quad - IR_{cell}(T) + U_p(SOC_p) - U_n(SOC_n) \end{aligned} \quad (22)$$

5. Energy Balance For Cell Temperature

As the temperature distribution within the cell is not considered in the SPM, the energy balance for the cell temperature should be integrated [1,3,4,8,9,11,13].

$$mC_p \frac{dT}{dt} = I(\eta_n - \eta_p + IR_{cell}) - IT\left[\frac{\partial U_p}{\partial T} - \frac{\partial U_n}{\partial T}\right] - hA_{cell}(T - T_{amb}) \quad (23)$$

In Eq. (23), the first term $I(\eta_n - \eta_p + IR_{cell})$ is the irreversible heat generation. The second term $IT\left[\frac{\partial U_p}{\partial T} - \frac{\partial U_n}{\partial T}\right]$ is the reversible heat generated by entropy change and has a positive or negative value. The values are usually regressed with experimental data. The heat due to mixing and phase change is ignored because they are considered to be negligible [11]. The third term, $hA_{cell}(T - T_{amb})$, is the heat exchange with the ambient environment, which is expressed using the convective heat transfer coefficient based on Newton's cooling law. Here, the radiant heat is negligible compared to the heat exchanged by convection. $\frac{dU_j}{dT}$ is given as follows in [1]. The unit of $\frac{dU_j}{dT}$ is mV/K.

$$\frac{dU_p}{dT} = \frac{-0.19952 + 0.92837 \cdot SOC_p - 1.36455 \cdot SOC_p^2 + 0.61154 \cdot SOC_p^3}{1 - 5.66148 \cdot SOC_p + 11.47636 \cdot SOC_p^2 - 9.83431 \cdot SOC_p^3 + 3.04876 \cdot SOC_p^4} \quad (24)$$

Table 1. Cell parameters and specifications [1]

	j=p	j=n	Unit
S_j	1.1167	0.7824	m^2
R_j	8.5×10^{-6}	12.5×10^{-6}	m
$c_{s,max}$	51,410	31,833	mol/m^3
c_e	1,000	1,000	mol/m^3
$k_{0,j}$	6.6667×10^{-14}	1.764×10^{-11}	$m^{2.5}mol^{-0.5}s^{-1}$
$Ea_{k,j}$	58,000	20,000	J/mol
$D_{s,j}$	1.0×10^{-14}	3.9×10^{-14}	m^2/s
$Ea_{D,j}$	29,000	35,000	J/mol
hA_{cell}	0.085		J/(s·K)
m	0.055		kg
C_p	750		J/(kg·K)

$$\frac{dU_n}{dT} = \frac{0.00527 + 3.29927 \cdot SOC_n - 91.79326 \cdot SOC_n^2 + 1{,}004.91101 \cdot SOC_n^3 - 5{,}812.27813 \cdot SOC_n^4 + 19{,}329.75490 \cdot SOC_n^5 - 37{,}147.89470 \cdot SOC_n^6 + 38{,}379.18127 \cdot SOC_n^7 - 16{,}515.05328 \cdot SOC_n^8}{1 - 48.09287 \cdot SOC_n + 1{,}017.23480 \cdot SOC_n^2 - 10{,}481.80419 \cdot SOC_n^3 + 59{,}431.30001 \cdot SOC_n^4 - 195{,}881.64880 \cdot SOC_n^5 + 374{,}577.31520 \cdot SOC_n^6 - 385{,}821.16070 \cdot SOC_n^7 + 165{,}705.85970 \cdot SOC_n^8} \quad (25)$$

SENSITIVITY ANALYSIS

The ODEs in Eqs. (7), (8), and (23) are the governing equations for calculating the SOC, terminal voltage, and temperature of the battery cell. The parameters for the cell in [1] are used and are listed in Table 1. The internal resistance parameter values according to the ambient temperature and current are listed in Table 2.

Using the parameters listed in Tables 1 and 2, we first simulate the cell under several C-rates and ambient temperatures to con-

Table 2. Parameter values for resistance according to ambient temperature and current [1]. 1C denotes the current that charge or discharge the battery cell in 1h. Here, 1C is equal to 1.656A because the nominal capacity is 1.656Ah. 1/2C represents half of 1C

Temperature (K)	Applied current		
	1/33C	1/2C	1C
288.15	θ_1=0.0789 Ω/K θ_2=0.0183 Ω/K	θ_1=0.0473 Ω/K θ_2=0.0188 Ω/K	θ_1=0.0150 Ω/K θ_2=0.0222 Ω/K
298.15	θ_1=0.0635 Ω/K θ_2=0.0233 Ω/K	θ_1=0.0392 Ω/K θ_2=0.0199 Ω/K	θ_1=0.0137 Ω/K θ_2=0.0159 Ω/K
308.15	θ_1=0.0116 Ω/K θ_2=0.0484 Ω/K	θ_1=0.0085 Ω/K θ_2=0.0428 Ω/K	θ_1=0.0056 Ω/K θ_2=0.0363 Ω/K
318.15	θ_1=0.0036 Ω/K θ_2=0.0495 Ω/K	θ_1=0.0049 Ω/K θ_2=0.0398 Ω/K	θ_1=0.0061 Ω/K θ_2=0.0298 Ω/K

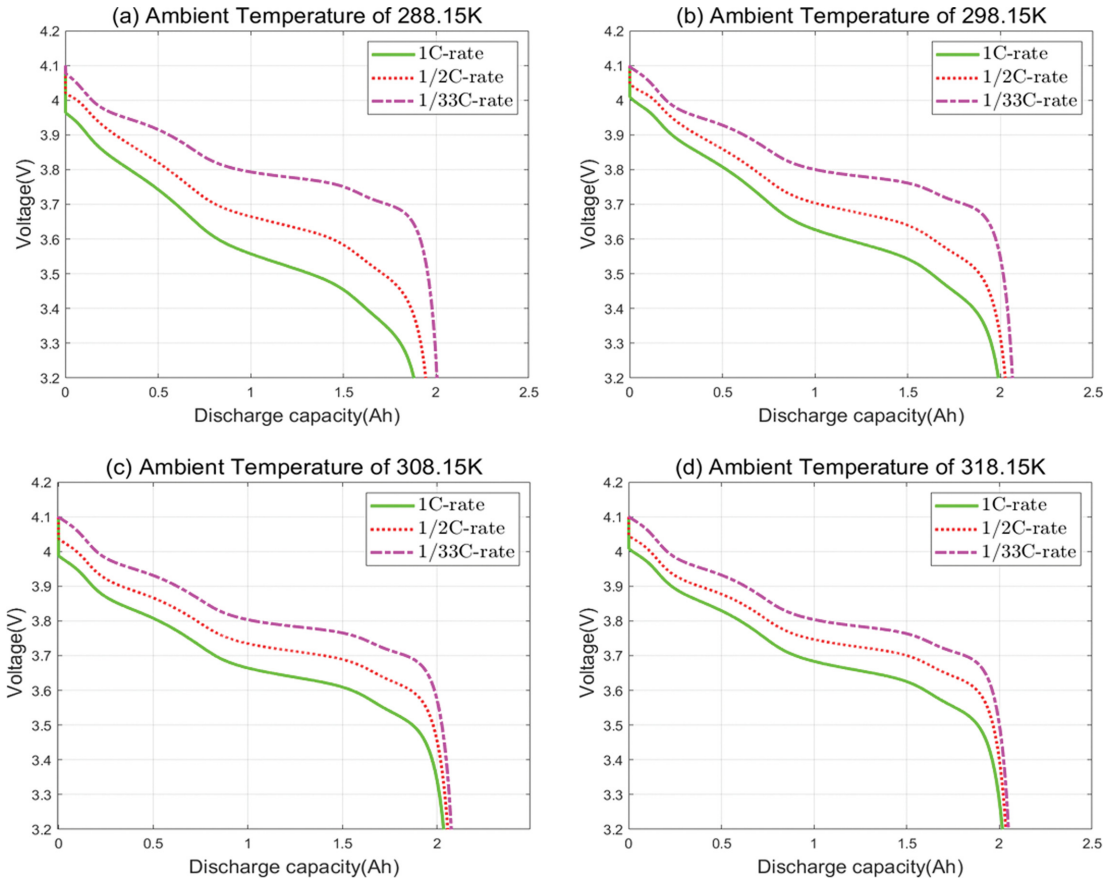

Fig. 2. Terminal voltage when discharging at 1 C, 1/2 C, and 1/33 C-rate until the cutoff-voltage of 3.2 V under the ambient temperatures (a) 288.15 K, (b) 298.15 K, (c) 308.15 K, and (d) 318.15 K.

firm the model compatibility and to investigate what factors are important for sensitivity analysis. The terminal voltage of the cell under 1C, 1/2C, and 1/33C is shown in Fig. 2. For Figs. 2(a), (b), (c), and (d), the ambient temperatures are set as 288.15 K, 298.15 K, 308.15 K, and 318.15 K, respectively. The discharge is simulated up to a cut-off voltage of 3.2 V to prevent damage owing to excessive discharge. The actual discharge capacity of the cell is calculated as follows:

$$\text{Discharge capacity (Ah)} = \frac{1}{3{,}600}\int_0^t \mathrm{I(s)ds}. \tag{26}$$

According to Fig. 2, the lower the ambient temperature, the faster the battery voltage reaches the cut-off voltage. As the average temperature inside the battery cell decreases, the chemical activity of the components participating in the reaction decreases. This results in a large voltage drop, and thus the actual discharge capacity decreases. This characteristic is well reflected by the diffusion coefficient of Eq. (5) and the reaction rate constant of Eq. (14). Therefore, under the ambient temperature of 288.15 K, the actual discharge capacity until the cut-off voltage is smaller than under other temperatures 298.15-318.15 K. This actual discharge capacity is one of the important factors to be the criterion for the sensitivity, which represents the trend of voltage drop.

The cell temperature is shown in Fig. 3(a) when the ambient temperature is 298.15 K and the constant C-rates of 1C, 1/2C, and 1/33C are applied. In Fig. 3(b), the temperature is plotted when the constant 1C-rate is applied under various ambient temperatures.

As shown in Fig. 3(a), the cell temperature increases when a large current is applied. The first term $\mathrm{I}(\eta_n - \eta_p + \mathrm{IR}_{cell})$ of Eq. (23) represents the amount of irreversible heat generation. The second term $-\mathrm{IT}[\partial \mathrm{U}_p/\partial \mathrm{T} - \partial \mathrm{U}_n/\partial \mathrm{T}]$ is the endothermic or exothermic quantity due to the reversible reaction. At the first few steps, the amount of absorbed and emitted heat is larger than the amount of heat generated; thus, there is fluctuation in temperature. Subsequently, the irreversible term for heat generation becomes much dominant compared to the reversible term and the amount that escapes to the outside; thus, the temperature increases. Owing to the $\mathrm{I}^2\mathrm{R}_{cell}$, which is the dominant term, the average temperature of the battery increases as the applied current increases. In the case of the 1/33 C-rate, the cell temperature rarely increases because the current load is negligible. As shown in Fig. 3(b) with the same C-rates at various ambient temperatures, the trend of change in the battery temperature is similar. The maximum temperature during the discharge can be selected as the criterion for the sensitivity when the initial temperature is set as the same, which represents the temperature changes.

In the following subsections, we will show the sensitivity results focusing on the discharge capacity and the maximum temperature under a constant 1C-rate discharge process at the ambient temperature of 298.15 K. For 16 variables in Table 1 except for mass m and specific heat capacity C_p, the effect on actual usable capacity and maximum temperature is analyzed. m and C_p are usually provided by battery suppliers. The regressions regarding the open circuit voltage are constructed separately with the OCV and Q-OCV tests. In addition, the parameters for the internal resistance can be obtained separately with pulse tests. Thus, we exclude them in the sensitivity analysis. The values shown in Table 1 are used as reference values, and the simulations are performed by multiplying the reference values by 0.8, 0.9, 1.1, and 1.2. Then, the percent change in the actual usable capacity and the maximum battery temperature is calculated.

When we perturb each parameter by ±10% and 20% and the capacity or maximum temperature changes by more than 1% of the reference values, the parameter is classified as a dominant parameter. By contrast, if a parameter is perturbed by ±10% and 20% and does not affect the capacity or maximum temperature by at least 1%, then the parameter is classified as a minor parameter. This implies that even with a large error in the minor parameter, only 1% error occurs in the simulation results. The errors in the minor parameter can be tolerated, and the priority of parameter estimation for dominant parameter is high. In addition, it is difficult to discriminate inaccuracy in the minor parameter estimates using the constant C-rate data. This implies that estimating the minor parameter from the constant C-rate data is not recommended.

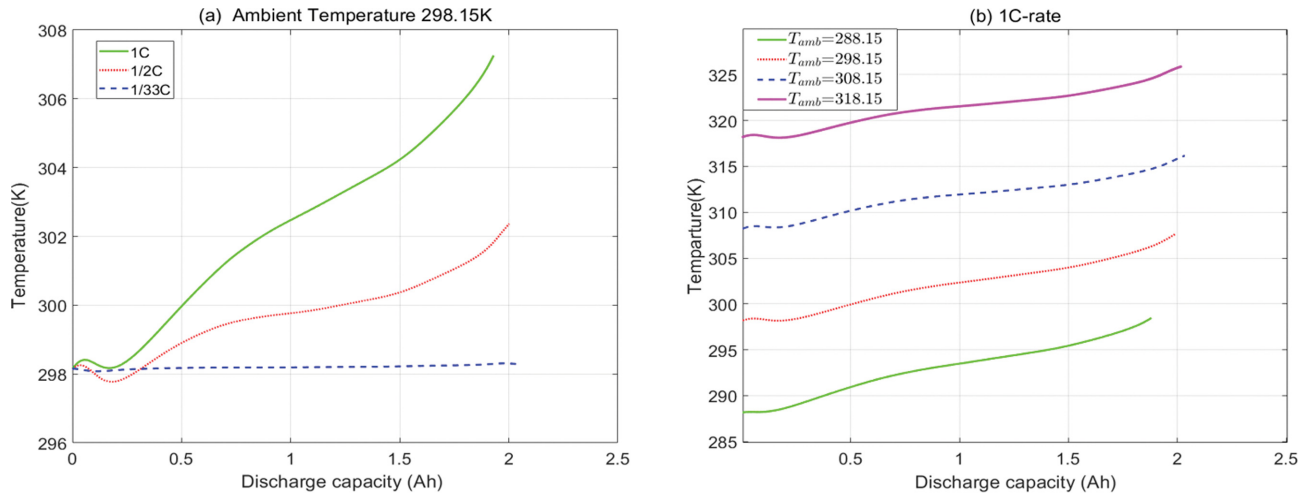

Fig. 3. (a) Cell temperature when various C-rates are applied, and the ambient temperature is 298.15 K. (b) Cell temperature at various ambient temperatures when 1C-rate is applied.

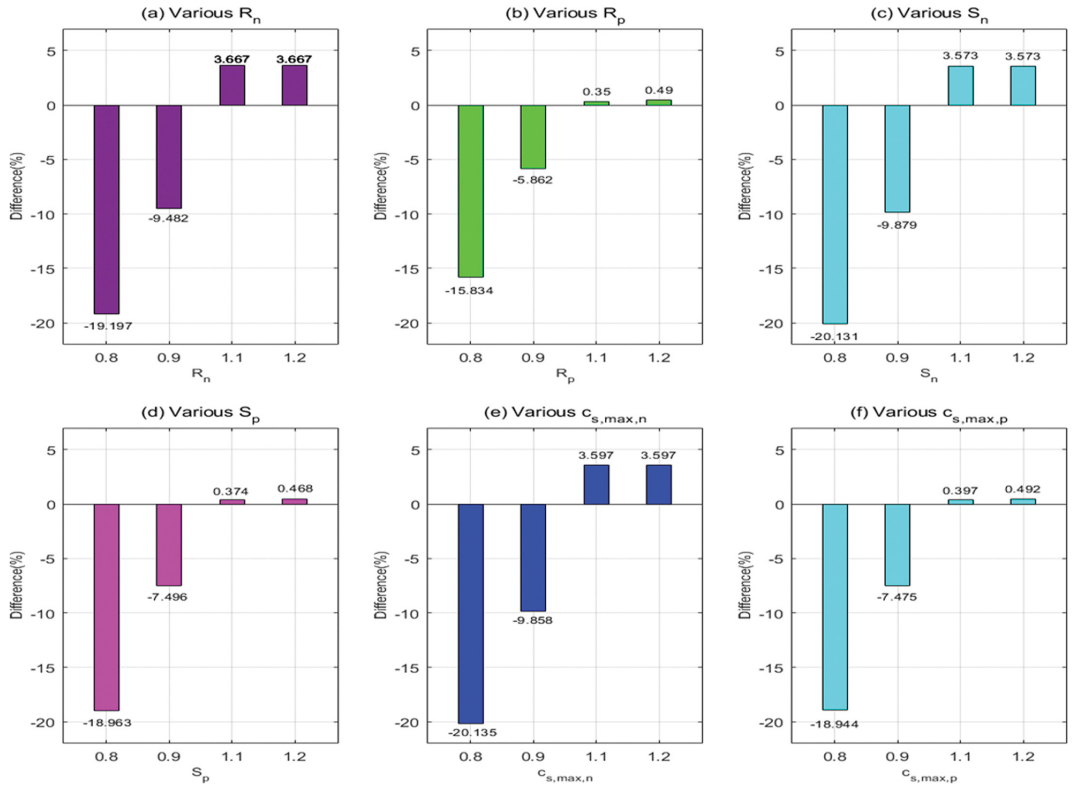

Fig. 4. Capacity sensitivity results of dominant parameters. Percent change in actual capacity under perturbed (a) R_n, (b) R_p, (c) S_n, (d) S_p, (e) $c_{s,max,n}$, and (f) $c_{s,max,p}$.

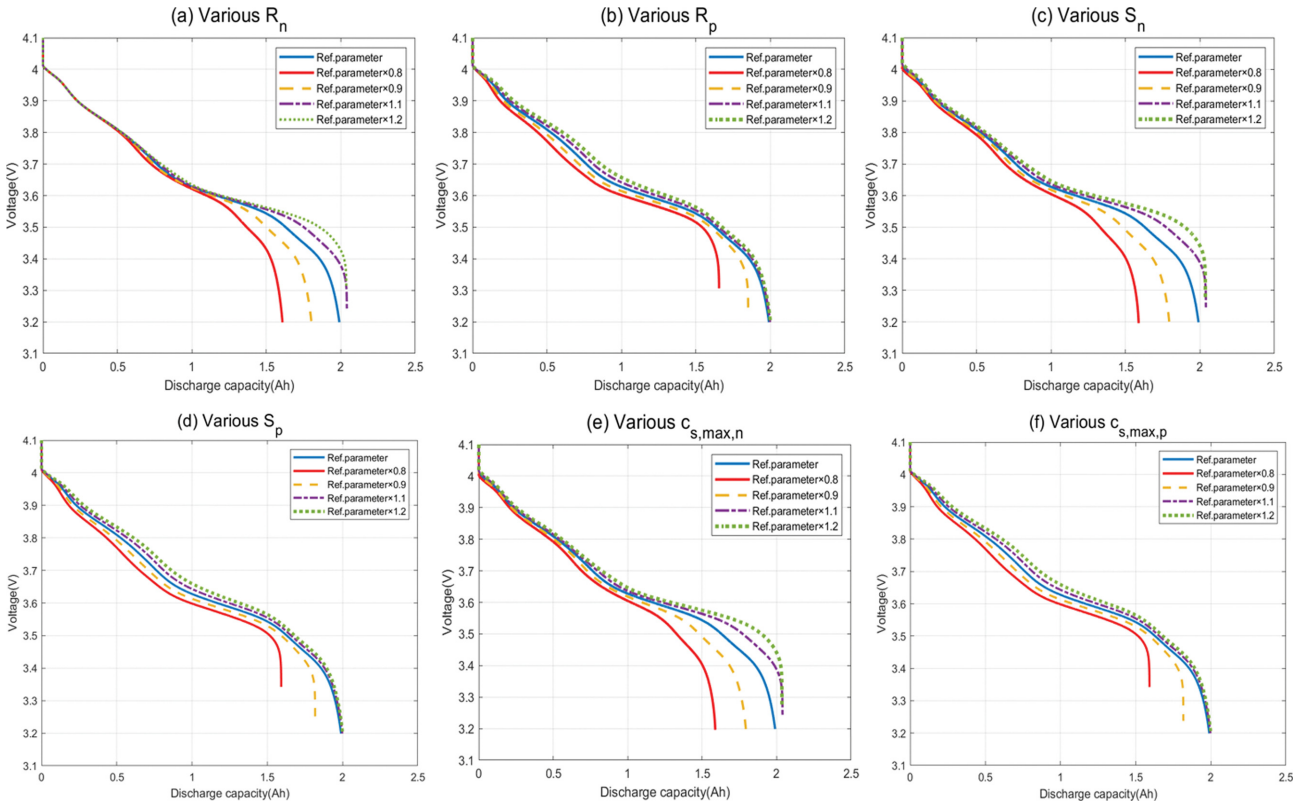

Fig. 5. Capacity sensitivity results of dominant parameters. Terminal voltage change under perturbed (a) R_n, (b) R_p, (c) S_n, (d) S_p, (e) $c_{s,max,n}$, and (f) $c_{s,max,p}$.

1. Sensitivity on Actual Usable Discharge Capacity

1-1. Dominant Parameters for Actual Usable Capacity

The results of the sensitivity analysis of R_n, R_p, S_n, S_p, $c_{s,max,n}$, and $c_{s,max,p}$ are shown in Figs. 4 and 5.

According to Figs. 4 and 5, six parameters dominantly affect the actual discharge capacity, and the effects appear in the terminal voltage, which is the main measurement. Shown in Figs. 4(a) and 5(a), as the radius of the anode R_n decreases, a large voltage drop occurs, resulting in a significant decrease in the discharge capacity. This is because the lithium-ion in the anode decreases fast based on Eq. (7) and accordingly, the surface concentration decreases rapidly. Fig. 5(c) shows the results perturbing the total active surface part of the anode. The smaller the active surface, the greater the molar flux on the surface, as described in Eq. (3). As a result, the concentration at the electrode surface drops sharply and the cut-off voltage is quickly reached. Therefore, the actual discharge capacity is significantly reduced. As the maximum concentration of the anode $c_{s,max,n}$ decreases, the exchange current $i_{0,n}$ of Eq. (16) decreases. It causes a large voltage drop to achieve the same 1C-rate. Thus, as shown in Figs. 4(e) and 5(e), the actual usable capacity decreases when $c_{s,max,n}$ decreases.

Figs. 4(b), 4(d), 5(b), and 5(d) show that when the radius R_p and the total active surface area S_p of the cathode decrease separately, the capacity significantly decreases. Like the anode, the amount capable of accommodating lithium ions decreases rapidly. The maximum amount of lithium ions that can be accommodated is reached even before the cutoff voltage. As a result, the actual discharge capacity is also reduced. As the parameters of the cathode increase, the amount capable of accommodating lithium ions increases. Thus, the actual discharge capacity increases as shown in Fig. 5(f). However, the amount of anode providing lithium ions remains unchanged, and thus the effects are smaller than when the parameters decrease.

1-2. Minor Parameters for Actual Usable Capacity

The sensitivity results for the minor parameters are as follows.

According to Figs. 6 and 7, ten parameters have minor effects on the actual capacity: the electrolyte concentration $c_{e,o}$, the convective heat transfer coefficient h, the diffusion rate coefficients $D_{s,n}$, $D_{s,p}$, the reaction rate coefficients $k_{o,n}$, $k_{o,p}$, the activation energies of diffusion $E_{a_{d,n}}$, $E_{a_{d,p}}$, and the activation energies of reaction, $E_{a_{k,n}}$, $E_{a_{k,p}}$.

Considering Eqs. (15), (16), and (22), as the electrolyte concentration c_e decreases, the overpotential drop increases owing to the decrease in the exchange current $i_{o,j}$. Thus, the actual usable capac-

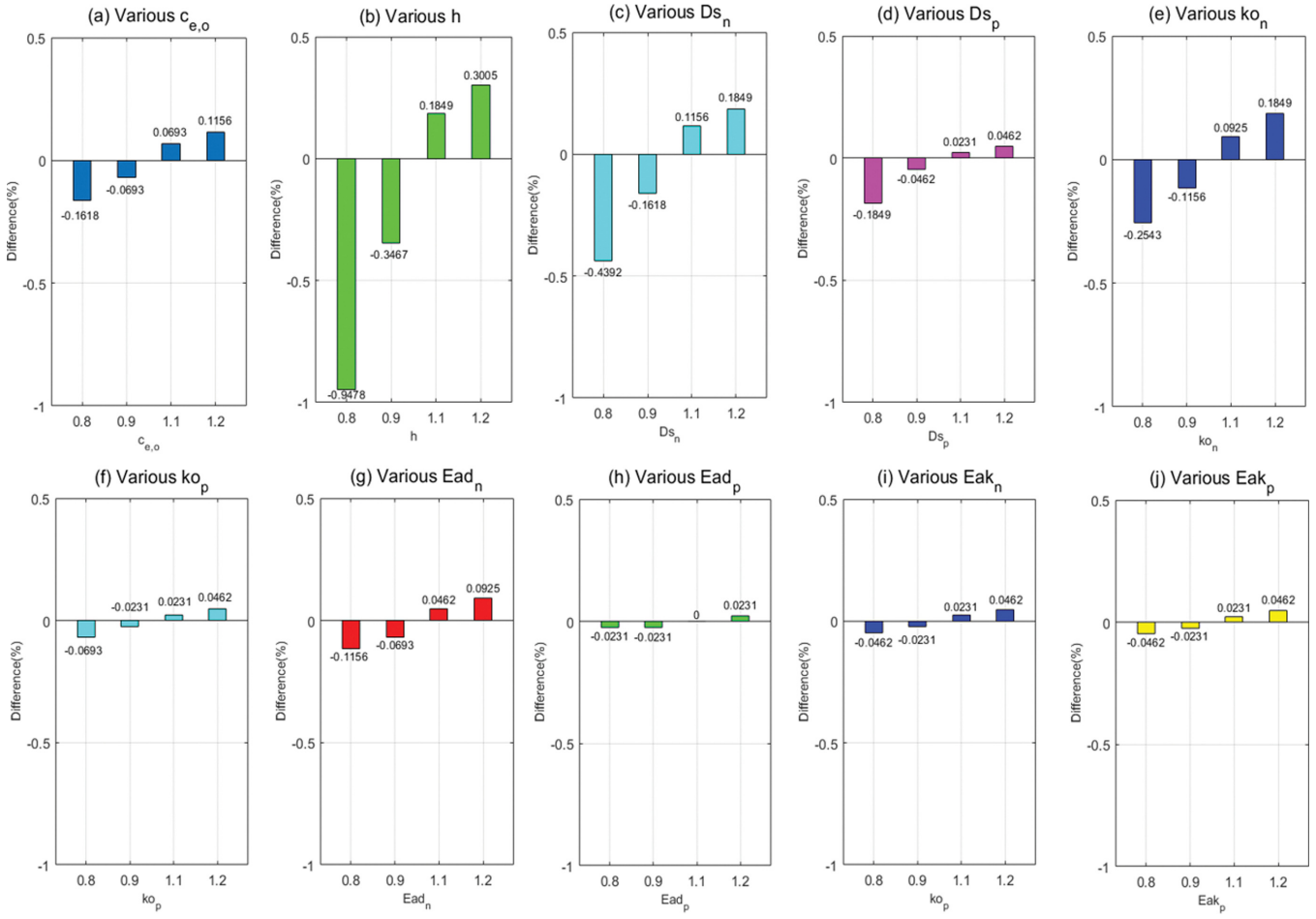

Fig. 6. Capacity sensitivity results of minor parameters. Percent change in actual capacity under perturbed (a) $c_{e,o}$, (b) h, (c) $D_{s,n}$, (d) $D_{s,p}$, (e) $k_{o,n}$, (f) $k_{o,p}$, (g) $E_{a_{d,n}}$, (h) $E_{a_{d,p}}$, (i) $E_{a_{k,n}}$, and (j) $E_{ak,p}$.

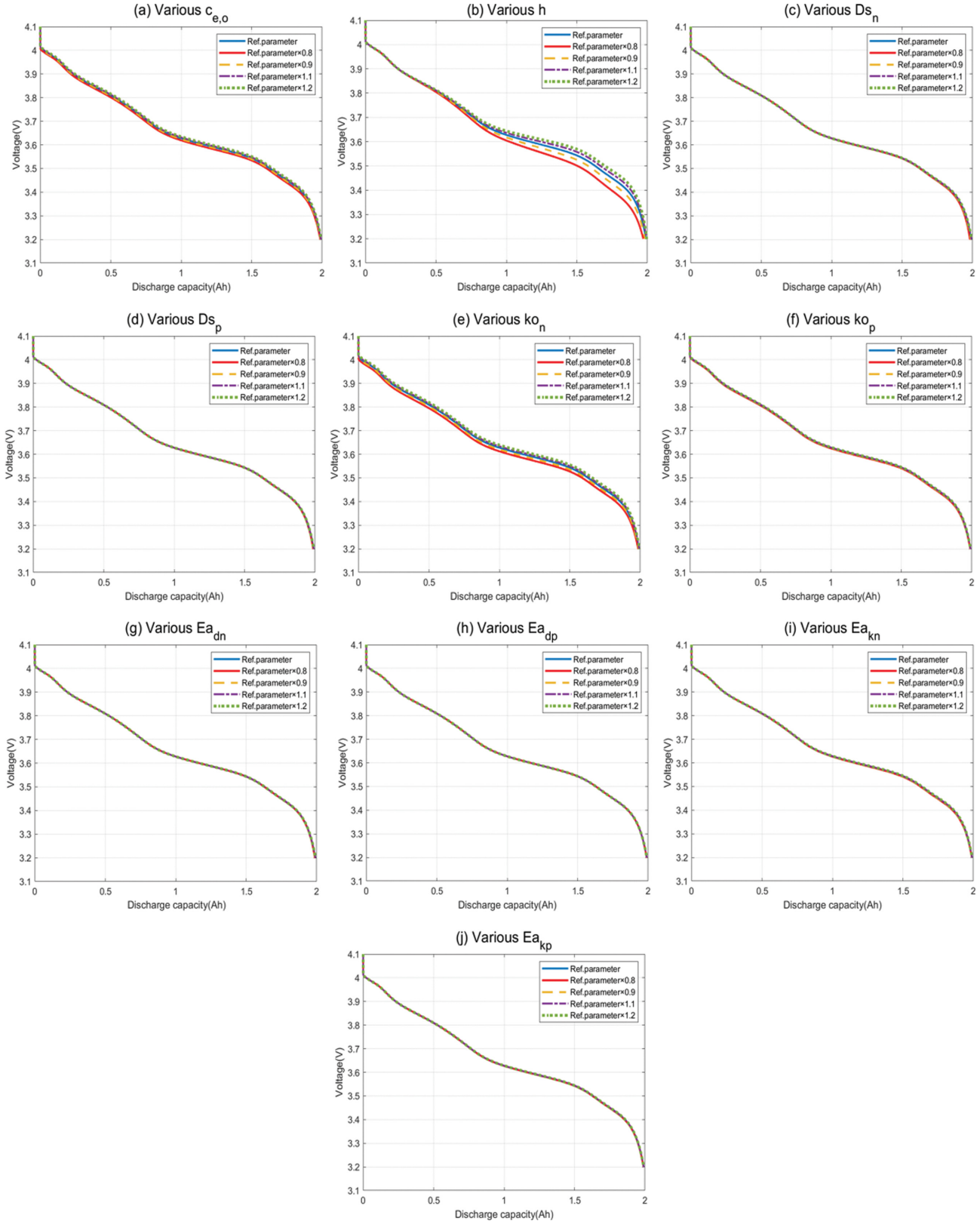

Fig. 7. Capacity sensitivity results of minor parameters. Terminal voltage change under perturbed (a) $c_{e,o}$, (b) h, (c) $D_{s,n}$, (d) $D_{s,p}$, (e) $k_{o,n}$, (f) $k_{o,p}$, (g) $E_{a_{d,n}}$, (h) $E_{a_{d,p}}$, (i) $E_{a_{k,n}}$, and (j) $E_{a_{k,p}}$.

ity decreases because the terminal voltage reaches the cut-off voltage rapidly (Fig. 6(a)). Here, note that j_p is negative and j_n is positive when discharging. Conversely, as $c_{e,o}$ increases, the overpotential drop decreases owing to an increase of $i_{o,j}$. Accordingly, the dis-

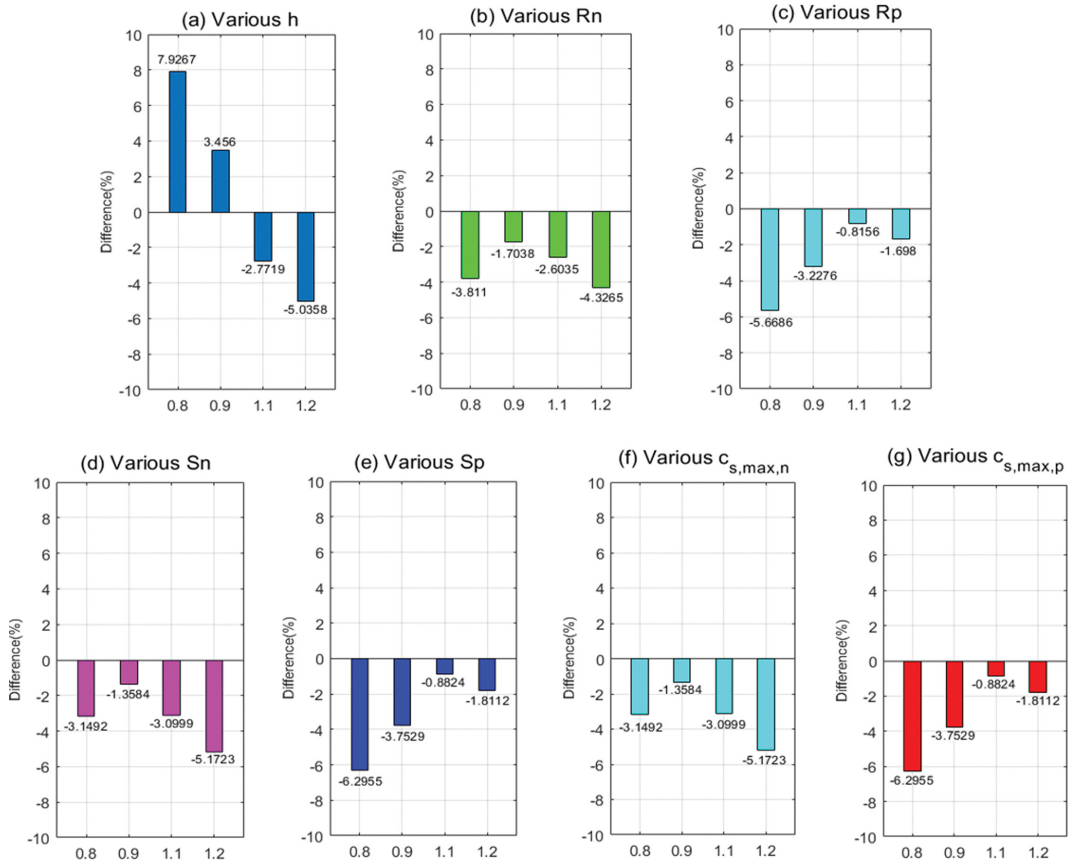

Fig. 8. Temperature sensitivity results of dominant parameters. Percent change in maximum temperature under perturbed (a) h, (b) R_n, (c) R_p, (d) S_n, (e) S_p, (f) $c_{s,max,n}$, (g) $c_{s,max,p}$.

charge capacity increases. However, the effect on the terminal voltage and the change in the actual capacity are insignificant under constant C-rate.

As shown in Fig. 6(b), the convective heat transfer coefficient h has the most significant influence among the minor parameters. The change in actual discharge capacity is because the amount of heat emitted to the outside is changed with h. The effect of h needs to be discussed with its effect on the temperature, which will be handled in the next subsection.

Because lithium ions move from the negative electrode to the positive electrode during discharging, the diffusion coefficient $D_{s,j}$ and the reaction rate coefficient $k_{o,j}$ affect the actual discharge capacity. When the values decrease separately, the absolute values of overpotential increase because of the decrease in the reaction and diffusion rates; thus, the voltage drop increases and the actual capacity decreases (Figs. 6(c)-(f)). Here note that the overpotentials of cathode and anode are negative and positive, respectively. The diffusion rate activation energy $E_{a_{k,j}}$ and reaction rate activation energy $E_{a_{d,j}}$ have the least sensitivity; thus, the difference in the terminal voltage from the reference result is quite small, as shown in Figs. 7(g), (h), (i), and (j).

2. Temperature Sensitivity

2-1. Dominant Parameters for the Temperature

Using the same simulation results, we calculate the percent change in the maximum temperature during the simulation. Consequently, there are seven dominant parameters for temperature, and the results are as follows:

Figs. 8 and 9 show that the dominant parameters regarding capacity are also dominant to the temperature. In addition, h significantly affects the maximum temperature, as shown in Figs. 8(a) and 9(a). R_j decreases, then the maximum temperature during the simulation decreases compared to the results under the reference value. Each decrease of S_j and $c_{s,max,j}$ gives the same trends on the maximum temperature. This is because the decrease of each parameter causes an increase of overpotential drop, as shown in Fig. 5. Subsequently, the cut-off voltage is reached earlier than in the reference case. Thus, the maximum temperature decreases because of the short discharge duration. When R_j, S_j and $c_{s,max,j}$ increase, the overpotential drop decreases, as shown in Fig. 5. The irreversible exothermic term decreases with a smaller overpotential drop; thus, the maximum temperature decreases compared with the reference case.

2-2. Minor Parameters for the Temperature

The minor parameter results for temperature are as follows:

Figs. 10 and 11 show that most of the minor parameters for capacity are also minor parameters for the temperature. Among the minor parameters, the electrolyte concentration $c_{e,o}$ and the reaction rate coefficient of the negative electrode $k_{o,n}$ have some sensitivity compared to the others. The other parameters show very small changes in temperature from the reference results. As $c_{e,o}$ decreases,

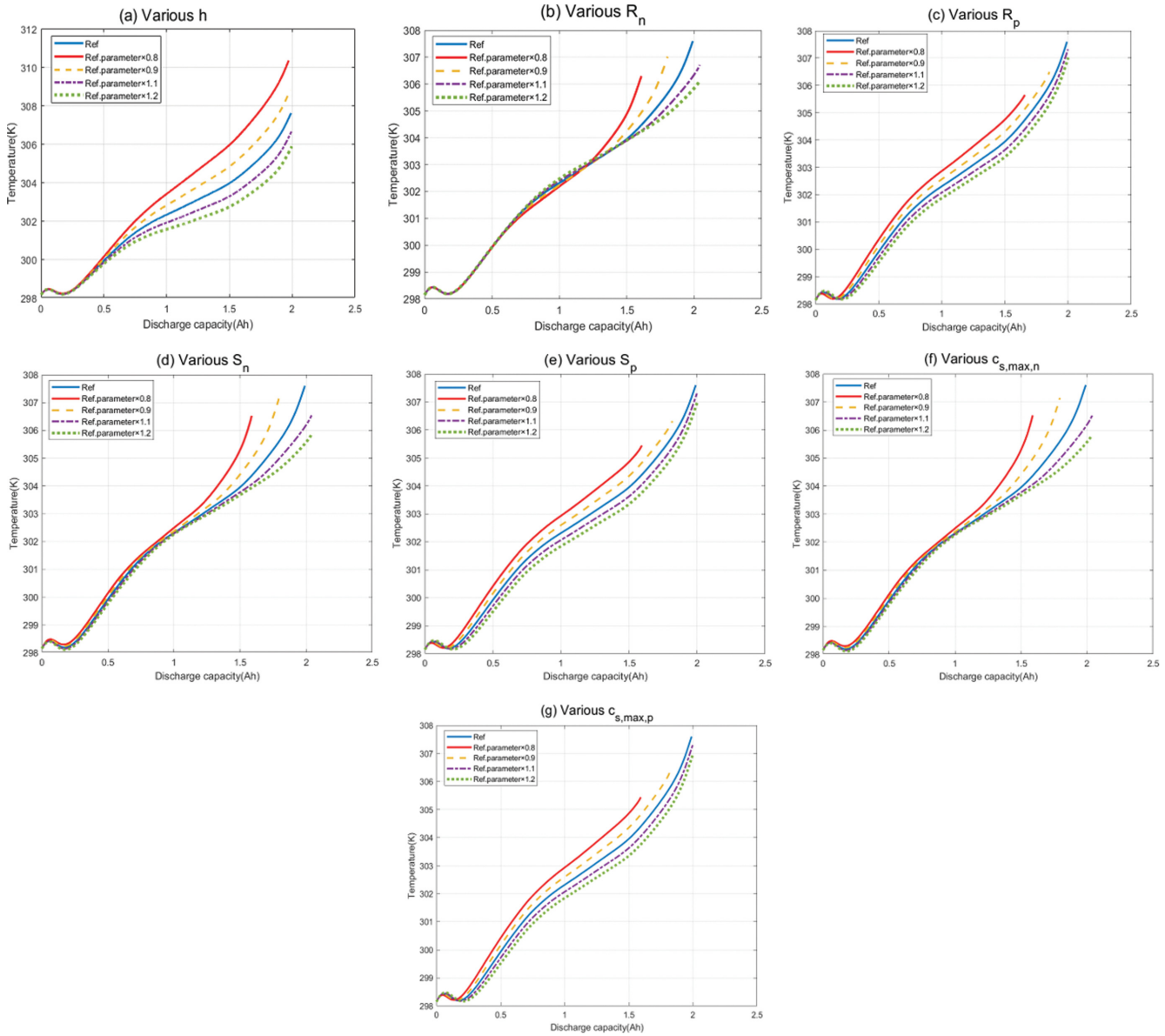

Fig. 9. Temperature sensitivity results of major parameters. Temperature change under perturbed (a) h, (b) R_n, (c) R_p, (d) S_n, (e) S_p, (f) $c_{s,max,n}$, (g) $c_{s,max,p}$.

the amount of lithium ions that can participate in the reactions is decreased. Accordingly, the exchange current is decreased, then overpotential drop is increased compared with the reference case. Thus, the irreversible calorific value is increased, and the temperature of the cell is increased. However, from Figs. 10(a) and 11(a), the maximum temperature of the cell increases only by 0.4325% than the reference case. Among the minor parameters, $k_{o,n}$ has the most significant influence. As $k_{o,n}$ decreases, the exchange current decreases owing to the decrease in the reaction rate; thus, the amount of heat generated increases owing to the increase in overpotential drop. However, $k_{o,n}$ also shows that the temperature of the cell increases only by 0.7547% because the overpotential drop increases slightly, as illustrated in Fig. 6(e).

From Figs. 4 and 8, there are seven dominant parameters in SPM integrated with energy balance: radius R_j, total active area S_j, the maximum concentration of the electrode $c_{s,max,j}$, and convective heat transfer coefficient h. Dominant parameters have a significant influence on the battery voltage, actual discharge capacity, and temperature; thus, a slight change in the dominant parameters changes the result significantly. Therefore, it is possible to estimate the dominant parameters accurately from the constant C-rate experimental data. The sensitivity effects on the accuracy of parameter estimation are described in the next section.

PARAMETER ESTIMATION

In this section, the dominant and minor parameters are estimated to evaluate the influence of parameter sensitivity on the accuracy of parameter estimation. The simulation results obtained by using the reference parameters under the ambient temperature of

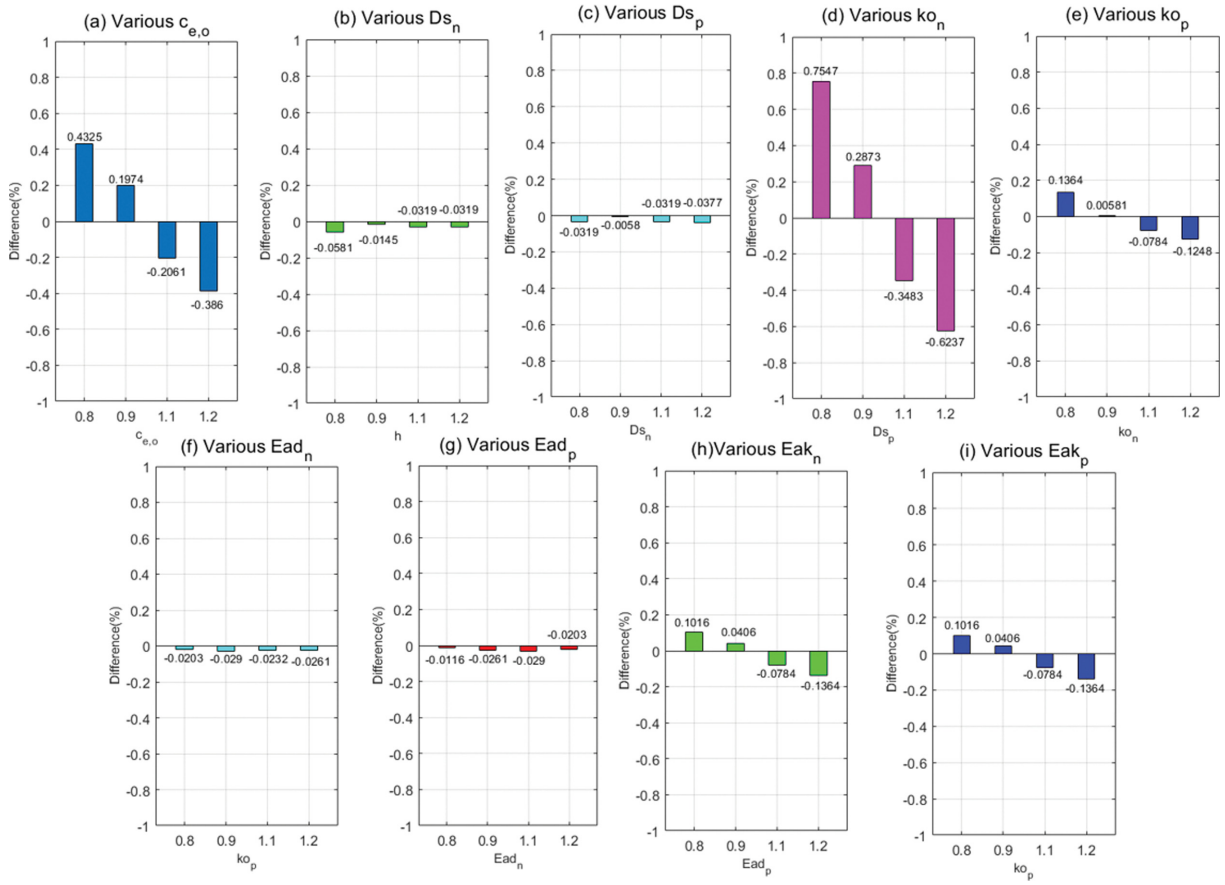

Fig. 10. Temperature sensitivity results of minor parameters. Percent change in maximum temperature under perturbed (a) $c_{e,o}$, (b) $D_{s,n}$, (c) $D_{s,p}$, (d) $k_{o,n}$, (e) $k_{o,p}$, (f) $E_{a_{d,n}}$, (g) $E_{a_{d,p}}$, (h) $E_{a_{k,n}}$, and (i) $E_{a_{k,p}}$.

298.15 K and 1C-rate discharge are assumed to be virtual experimental data. The reason for using the virtual experimental data is that when the actual experimental data are used, the true parameter values are unknown and the parameter estimation accuracy cannot be investigated. We used MATLAB for simulation and parameter estimation. In particular, the genetic algorithm (GA) was used for parameter estimation.

1. Dominant Parameter Estimation

Among the dominant parameters, R_n, R_p, S_n, and S_p are estimated. The actual maximum lithium-ion concentration can be obtained by measuring the mass and volume change of each electrode at the fully charged and fully discharged conditions from the initial states of the anode and cathode. Because h changes depending on the air or coolant flow rate, h is not estimated herein.

The parameter estimation problem is shown in Eq. (27) with the notation $\dot{x}=f(x; p)$ for the governing equations. p represents the normalized parameter vector where the maximum and minimum values are set as 0.5 and 1.5 of the reference parameters. Thus, p is bounded with the all-ones and all-zeros vectors. The objective function J(p) includes the mean squared errors of the terminal voltage and the temperature. Note that each term is scaled by the variances of experimental data. The maximum temperature difference is additionally considered to give more weights on the battery temperature accuracy. t_{total} is the total discharge time and the subscription exp denotes the virtual experimental data.

Table 3. Estimated value of dominant parameters. Percent error in the estimates with respect to the true values

Parameter	Estimated value	Percent error (%)
R_p	8.2395×10^{-6}	−3.065
R_n	12.471×10^{-6}	−0.23
S_p	1.1468	2.695
S_n	0.7845	0.265

$$\min_p J(p)=\frac{1}{t_{total}}\left(\sum_{t=1}^{t_{total}}\frac{(V(t)-V_{exp}(t))^2}{Var(V_{exp})}+\sum_{t=1}^{t_{total}}\frac{(T(t)-T_{exp}(t))^2}{Var(T_{exp})}\right)+Max(T-T_{exp})$$

$$\text{subjecto to } \dot{x}=f(x; p), \quad 0\le p\le 1 \tag{27}$$

The estimated values for the parameters and the percent error in the estimates with respect to the true values are shown in Table 3. Because we use the virtual experimental data generated using the reference values, the true values of the parameters are the reference values. The absolute percent error in the estimates regarding the true values is smaller than 3.1%. The simulation results with the estimated parameters are compared with the reference results, which are shown in Fig. 12. The percent errors in actual usable discharge capacity and maximum temperature are shown in Table

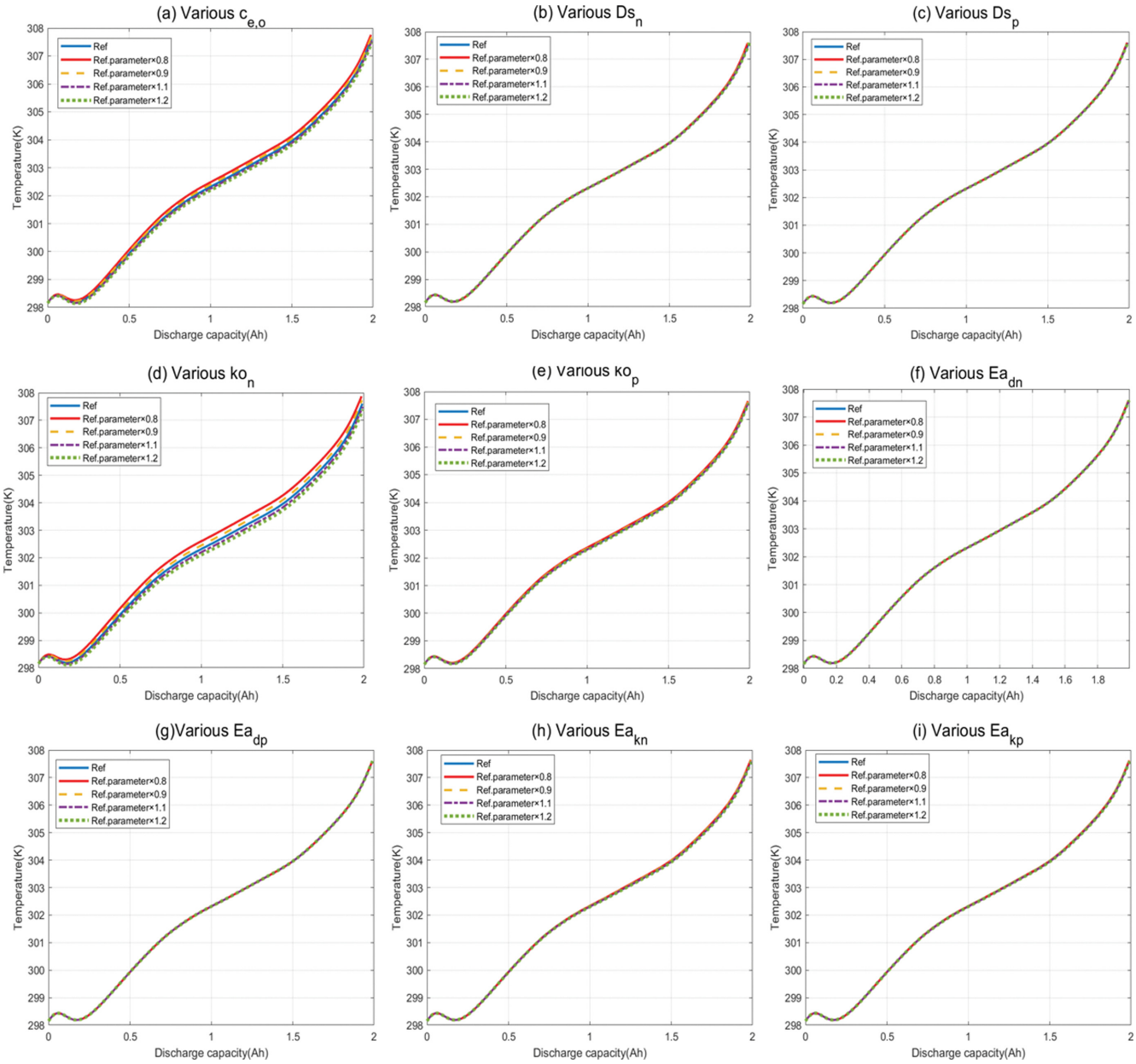

Fig. 11. Temperature sensitivity results of minor parameters. Temperature changes under perturbed (a) $c_{e,o}$, (b) $D_{s,n}$, (c) $D_{s,p}$, (d) $k_{o,n}$, (e) $k_{o,p}$, (f) $E_{ad,n}$, (g) $E_{ad,p}$, (h) $E_{ak,n}$, and (i) $E_{ak,p}$.

Table 4. Percent error in actual usable capacity and maximum temperature when conducting simulation with the estimated dominant parameters

	Actual usable capacity	Maximum temperature
Percent error (%)	−0.0275	−0.0261

4. The absolute values of the percent errors in the capacity and maximum temperature are both smaller than 0.03%.

To validate the estimated parameters, we also apply a hybrid pulse power characterization (HPPC) test scenario where the discharge at 1C-rate and the rest are repeated. The simulation results with the estimated parameters and the reference values are shown in Fig. 13. In Table 5, the error percentages in the actual capacity and the maximum temperature are shown, which are only 0.0109% and −0.0248%, respectively. Owing to the high sensitivity, the dominant parameters are estimated accurately from the constant C-rate experimental data.

Table 5. Percent error in actual usable capacity and maximum temperature for the validation data (Dominant parameter)

	Actual usable capacity	Maximum temperature
Percent error (%)	0.0109	−0.0248

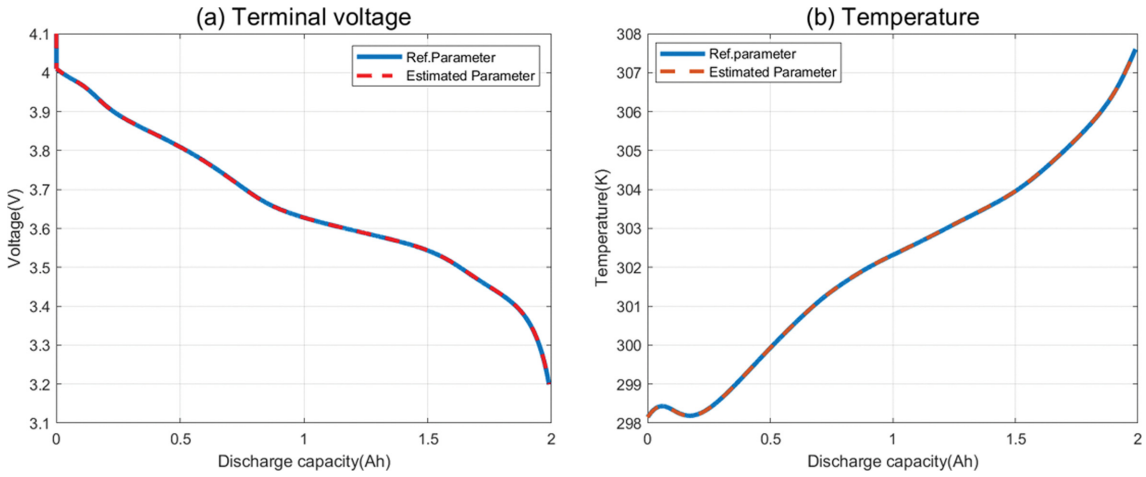

Fig. 12. (a) Voltage and (b) cell temperature results when simulated with the estimated parameters and with the reference values.

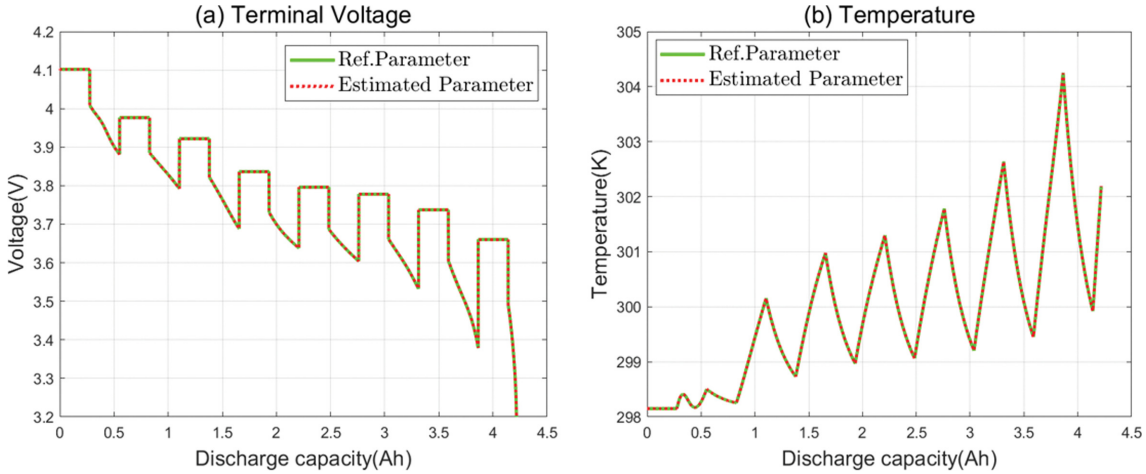

Fig. 13. Validation results of dominant parameter estimation. (a) Voltage and (b) Cell temperature.

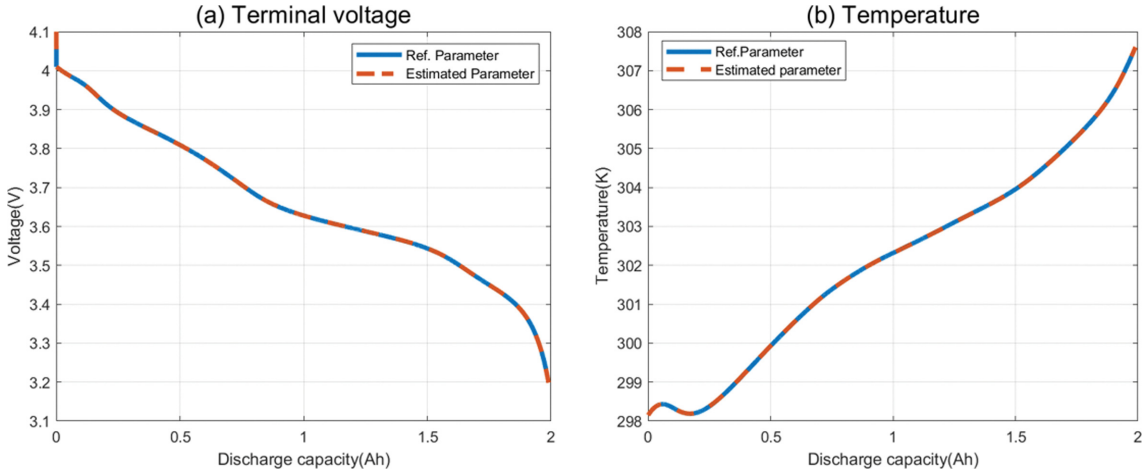

Fig. 14. Estimation results of minor parameters. (a) Voltage and (b) cell temperature results with the estimated parameters and with the reference values.

2. Minor Parameter Estimation

Ten minor parameters are estimated using GA. The estimated parameters and the percent error with respect to the reference values are summarized in Table 6. Fig. 14 shows the simulation results.

Table 6. Estimates of minor parameters. Percent error in the estimates with respect to the reference values

Parameter	Estimated value	Percent error (%)
$c_{e,p}$	986.9	−1.31
$c_{e,n}$	849.2	−15.08
$D_{s,p}$	9.37×10^{-15}	−6.305
$D_{s,n}$	4.454×10^{-14}	14.215
$k_{o,p}$	5.976×10^{-11}	−10.355
$k_{o,n}$	1.956×10^{-11}	10.885
$E_{a_{d,p}}$	31,883	9.94
$E_{a_{d,n}}$	25,328	−27.6350
$E_{a_{k,p}}$	56,353	−2.84
$E_{a_{k,n}}$	20,125	0.624

Table 7. Percent error in actual usable capacity and maximum temperature when simulating with the estimated values of minor parameters

	Actual usable capacity	Maximum temperature
Percent error (%)	0.0322	0.0029

In Table 7, the percent error in actual discharge capacity and maximum battery temperature are shown. Minor parameters have low sensitivity, and the effect on voltage and cell temperature is negligible, as illustrated in Figs. 7 and 11. It affects the estimation accuracy of the minor parameters. The percent error in the minor parameters is much greater than that for the dominant parameters; however, as shown in Fig. 14 and Table 7, it causes only small differences between the simulation results with the estimated parameters and those with the reference values. The error percentages in actual capacity and maximum temperature are only 0.0322% and 0.0029%, respectively.

The estimation values of the minor parameters are validated under the HPPC test with 1C-rate. The validation results are shown in Fig. 15 and Table 8. Even with estimates having large errors, the voltage and the temperature results are quite similar to those of the reference parameters.

Table 8. Percent error in actual usable capacity and maximum temperature for validation data (Minor parameter)

	Actual usable capacity	Maximum temperature
Percent error (%)	0.1360	−0.4373

The effects of the parameter changes on the measurements are small; thus, additional experiments are required to estimate the parameters with minor influence. The kinetic parameters and diffusion coefficient can be estimated using cyclic voltammetry and measuring the peak currents [17,18,20]. With a slow scan rate, a finite diffusion process occurs; thus, the diffusion rate limits the current so that the diffusion parameters can be estimated. The Randles-Sevcik equation is used to calculate the diffusion coefficient. In the region of a fast scan rate, a semi-infinite diffusion process dominates the peak current. Thus, the reaction rate is calculated using the peak current under the condition. To this end, Koutecky-Levich equation and Nicholson's method are used. The activation energy of reaction and diffusion rates can be estimated by conducting experiments under various temperatures. Separately, the galvanostatic intermittent titration technique, potentiostatic intermittent titration technique, and the current pulse relaxation method can also be used [17-21].

CONCLUSION

We identified the parameters that can be estimated with high accuracy from general and simple experimental results. First, the simplified single particle model (SPM) integrated with energy balance was constructed and investigated. From the simulation under various C-rates and ambient temperatures, we selected two main factors for the sensitivity analysis: actual capacity and maximum temperature. Second, through sensitivity analysis focusing on the factors, the parameters that significantly affect the measurements were identified. Third, we validated the estimation accuracy of those dominant parameters using the virtual experimental data.

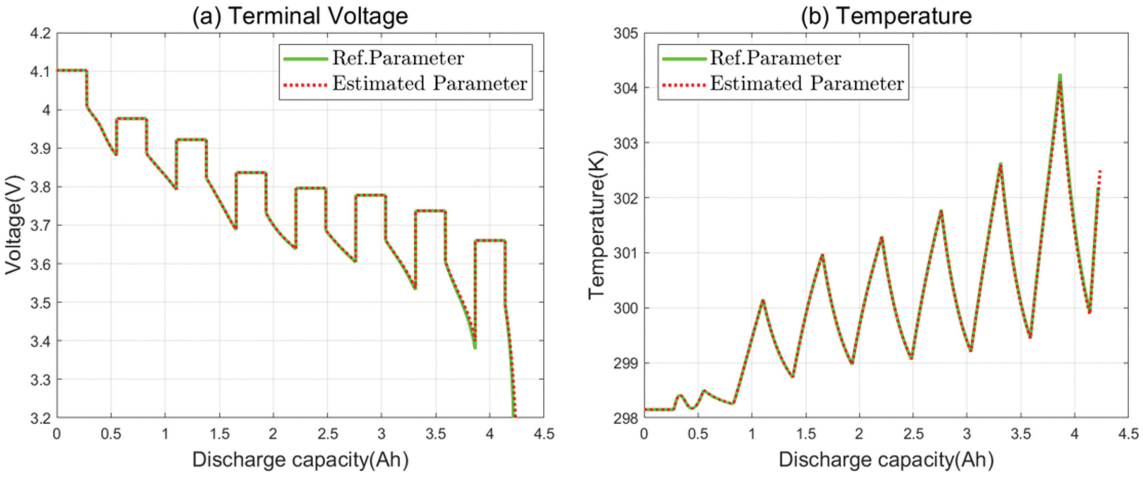

Fig. 15. Validation results of minor parameter estimation: (a) Voltage and (b) Cell temperature.

From the sensitivity analysis, there are seven dominant parameters for the actual capacity and temperature: radius R_j, total active area S_j, maximum electrode concentration $c_{s,max,j}$ of electrodes and convective heat transfer coefficient h. The parameters are estimated to be within 3.1% error using the 1C-rate virtual experimental data. Meanwhile, although minor parameters have large errors from the reference values, the differences in the voltage and temperature from the virtual experimental data obtained with the reference values are almost indistinguishable. Furthermore, the error percentages in the actual capacity and maximum temperature are only 0.1360% and −0.4373% for the validation data. Through this sensitivity analysis and the estimation results, we confirmed that the dominant parameters can be estimated sufficiently accurately from the constant C-rate experiments. Additional experiments such as cyclic voltammetry are required only for the minor parameters.

ACKNOWLEDGEMENTS

This work was supported by the National Research Foundation of Korea (NRF) grant funded by the Korea government (MSIT) (NRF-2021R1C1C1004217), and by Hyundai Motor Company as Development of Battery Thermal Model considering Battery Aging for Integrated Thermal Management. The present research has been conducted by the Research Grant of Kwangwoon University in 2020.

NOMENCLATURE

A_{cell} : total cell surface area exposed to surroundings [m^2]
C_p : specific heat capacity of the cell [J/kg·K]
$c_{s,max,j}$: maximum concentration of lithium ions *j* [mol/m^3]
$\bar{c}_j$: volume-averaged Li^+ concentration in the solid phase [mol/m^3]
$c_{s,j}$: Li^+ concentration at solid surface
$D_{s,j}$: electrolyte diffusivity coefficient in the solid phase [m^2/s]
$E_{a_{d,j}}$: activation energy for the solid-phase diffusion coefficient of electrode *j* [kJ/mol]
$E_{a_{r,j}}$: activation energy for the reaction rate constant of electrode *k* [kJ/mol]
F : faraday constant [96,487 C/mol]
j : Li^+ mole flux at solid surface [mol/m^2/s]
k_j : rate constant for the electrochemical reaction of electrode *j* [$m^{2.5}$/$mol^{0.5}$·S]
h : heat transfer coefficient between the cell and the surroundings [W/m^2·K]
Q : rate of heat transfer between the cell and surroundings [W]
$\bar{q}_j$: volume-average Li^+ concentration flux in the solid phase [mol/m^4]
S_j : total electroactive area of the electrode *j* [m^2]
R_j : radius of spherical intercalation of electrode *j* [m]
R : ideal gas constant [8.314 J/mol·K]
T : cell temperature [K]
T_{amb} : ambient temperature [K]
T_{ref} : reference temperature [298.15 K]
V : terminal voltage [V]
$\phi_{1,j}$: solid phase potential of electrode *j* [V]
$\phi_{2,j}$: solution phase potential of electrode *j* [V]

REFERENCES

1. M. Guo, G. Sikha and R. E. White, *J. Electrochem. Soc.*, **158**(2), A122 (2011).
2. V. R. Subramanian, V. D. Diwakar and D. Tapriyal, *J. Electrochem. Soc.*, **152**(10), A2002 (2005).
3. K. An, P. Barai, K. Smith and P. P. Mukherjee, *J. Electrochem. Soc.*, **161**(6), A1058 (2014).
4. Y. Choi and H. Kim, *Korean Ind. Chem.*, **18**(5), 47 (2015).
5. B. Wu, *J. Power Sources*, **243**, 544 (2013).
6. Y. Ma, *IEEE Access*, **7**, 156136 (2019).
7. K. Kumaresan, G. Sikha and P. E. White, *J. Electrochem. Soc.*, **155**(2), A164 (1993).
8. A. P. Schmidt, *IFAC Symposium Advances in Automotive Control*, **43**(7), 198 (2010).
9. M. Farag, H. Sweity, M. Fleckenstein and S. Habibi, *J. Power Sources*, **360**, 618 (2010).
10. R. Gu, *IEEE Transactions on Transportation Electrification*, **2**(4), 417 (2016).
11. D. Bernardi, E. Pawlikoski and J. Newman, *J. Electrochem. Soc.*, **132**(5), 5 (1985).
12. W. Li, *Appl. Energy*, **269**, 115104 (2020).
13. L. Zhang, *J. Electrochem. Soc.*, **161**(5), A762 (2014).
14. M. Chen and G. A. Rincón-Mora, *IEEE Transactions on Energy Conversion*, **21**(2), 504 (2006).
15. H. Pang, *Electrochm. Acta*, **307**, 474 (2019).
16. K. Jiang, *J. Power Sources*, **451**, 1 (2020).
17. F. Xue, *Electrochem. Acta*, **53**, 6636 (2008).
18. H. Wang, *ACS NANo*, **14**, 2575 (2020).
19. Z. Mao, M. Farkhondeh, M. Pritzker, M. Fowler and Z. Chen, *Electrochim. Acta*, **222**, 1741 (2016).
20. J. K. Park, *Principles and applications of lithium secondary batteries*, Wiley-VCH Verlag & Co. KGaA, Weinheim (2012).
21. J. J. Lee, *J. Korean Electrochem. Soc.*, **4**(4), 139 (2001).

APPENDIX

In Section 2.2., the SPM is further simplified by referring to [2, 10] before the energy balance is integrated. The lithium-ion concentration of the solid phase is considered as a fourth-order approximation in the radial direction, as in Eq. (6). This simplification can reduce the PDE of Eq. (1) into ordinary differential equations in Eqs. (7) and (8). Thus, the governing equations are simplified into the dynamics of the volume-averaged lithium-ion concentration of the solid phase $\bar{c}_j$ and lithium-ion concentration flux $\bar{q}_j$. For completeness, we briefly summarize the derivation of Eqs. (7)-(10).

The volume average concentration is as follows:

$$\bar{c}_j = \frac{1}{V_j}\int_0^{\pi}\int_0^{2\pi}\int_0^{R} c_{s,j}\, r^2 \mathrm{d}r \sin\theta \mathrm{d}\phi \mathrm{d}\theta \tag{A1}$$

Here, V_j is the volume of the single particle for each electrode, j. The time derivative of the volume-averaged solid-phase concentration is calculated by using Eq. (A2). The original mass balance in Eq. (1) and its boundary conditions in Eq. (2) are utilized to

obtain the dynamics of $\bar{c}_j$ as Eq. (7).

$$\frac{d\bar{c}_j}{dt} = \frac{1}{V_j}\int_0^{\pi}\int_0^{2\pi}\int_0^{R} \frac{\partial c_{s,j}}{\partial t} r^2 dr \sin\theta d\phi d\theta \quad (A2)$$

In addition, based on Eq. (A1) and the fourth-order approximate expression of $c_{s,j}$, the volume-averaged concentration is as follows:

$$\bar{c}_j(t) = \frac{3}{7}P(t) + \frac{3}{5}B(t) + A(t) \quad (A3)$$

The volume-averaged concentration flux term in Eq. (A4) is needed to fully define the original PDE,

$$\bar{q}_j(t) = \frac{1}{V_j}\int_0^{\pi}\int_0^{2\pi}\int_0^{R} \frac{\partial c_{s,j}}{\partial r} r^2 dr \sin\theta d\phi d\theta \quad (A4)$$

Substituting the fourth-order approximate expression of $c_{s,j}$ into Eq. (A4), we obtain

$$\bar{q}_j(t) = 2\frac{P(t)}{R_j} + \frac{3}{2}\frac{B(t)}{R_j} \quad (A5)$$

The time derivative of $\bar{q}_j(t)$, Eq. (8), is derived from Eq. (A6), which is obtained based on the fact that the original mass balance of Eq. (1) always holds.

$$\frac{1}{V_j}\int_0^{\pi}\int_0^{2\pi}\int_0^{R} \frac{\partial\left[\frac{\partial c_{s,j}}{\partial t} - D_s\frac{1}{r^2}\frac{\partial}{\partial r}\left(r^2\frac{\partial c_{s,j}}{\partial r}\right)\right]}{\partial r} r^2 dr \sin\theta d\phi d\theta = 0 \quad (A6)$$

The lithium-ion surface concentration is the concentration in the solid phase at $r=R_j$,

$$\bar{c}_{se,j} = c_{s,j}(R_j, t) = A(t) + B(t) + P(t) \quad (A7)$$

Finally, the time-varying constants, A(t), B(t), and P(t), are expressed as Eq. (10) by combining and rearranging Eqs. (A3), (A5), and (A7).